to CD3 (*20*). The T cell marker may be down-regulated after fusion with DCs, or the DCs may simply require contact with T cells to support viral replication.

Efforts can now be directed to determine whether DCs within the many lymphoid organs of the pharynx, collectively termed Waldeyer's ring, consistently represent a major site for HIV-1 replication early in disease. Infants who swallow virus from mothers during birth or breast feeding also may be infected initially in these tissues. Other extralymphoid sites in which DCs and T cells may interact and promote HIV-1 replication include inflamed genital surfaces and the afferent lymphatics that originate from just beneath the mucosa. Simian immunodeficiency virus DNA has been detected in presumptive DCs just beneath the uterine mucosa of monkeys that were acutely infected with the virus intravaginally (*24*). Further attention to tissues that contain interacting DCs and T cells may provide insight into critical sites for HIV-1 replication in situ.

## REFERENCES AND NOTES


1. D. D. Ho *et al.*, *Nature* **373**, 123 (1995).
2. X. Wei *et al.*, *ibid.*, p. 117.
3. K. Tenner Racz *et al.*, *Am. J. Pathol.* **123**, 9 (1986).
4. P. Biberfeld *et al.*, *ibid.* **125**, 436 (1986).
5. K. Tenner Racz *et al.*, *AIDS* **2**, 299 (1988).
6. P. U. Cameron, R. L. Dawkins, J. A. Armstrong, E. Bonifacio, *Clin. Exp. Immunol.* **68**, 465 (1987).
7. H. J. Schuurman, W. J. Krone, R. Broekhuizen, J. Goudsmit, *Am. J. Pathol.* **133**, 516 (1988).
8. C. H. Fox *et al.*, *J. Infect. Dis.* **164**, 1051 (1991).
9. J. Embretson *et al.*, *Nature* **362**, 359 (1993).
10. B. Weiser *et al.*, *Proc. Natl. Acad. Sci. U.S.A.* **87**, 3997 (1990).
11. The specimens were negative for microorganism stains (Brown-Hopps tissue Gram stain, periodic acid–Schiff stain, Grocott's methenamine silver stain, Ziehl-Neelsen acid-fast stain) and for immunolabeling with antibodies to Epstein-Barr virus, herpes simplex virus, or cytomegalovirus.
12. Formalin-fixed, paraffin-embedded tissues were sectioned, stained with the Kal-1 monoclonal antibody to HIV-1 p24 (DAKO) followed by peroxidase-avidin-biotin complex, and counterstained with hematoxylin.
13. K. Tenner Racz, P. Racz, M. Dietrich, P. Kern, *Lancet* i, 105 (1985); J. A. Armstrong and R. Horne, *ibid.* ii, 370 (1984); G. Pantaleo *et al.*, *Nature* **362**, 355 (1993).
14. M. Pope *et al.*, *Cell* **78**, 389 (1994); M. Pope, S. Gezelter, N. Gallo, L. Hoffman, R. M. Steinman, *J. Exp. Med.* **182**, 2045 (1995).
15. Keratin was identified with two specific monoclonal antibodies followed by alkaline phosphatase–conjugated secondary antibodies (DAKO). Antigens reactive with a monoclonal antibody to p24 and rabbit polyclonal antibodies to S100 (DAKO) were detected with a peroxidase reaction product.
16. K. Takahashi *et al.*, *Am. J. Pathol.* **116**, 497 (1984); H. J. Kahn, A. Marks, H. Thom, R. Baumal, *Am. J. Clin. Pathol.* **79**, 341 (1983).
17. J. Klein, *Immunology* (Blackwell, Boston, 1990), p. 52; D. W. Fawcett, *A Textbook of Histology* (Saunders, Philadelphia, 1986).
18. L. P. Ruco *et al.*, *J. Pathol.* **176**, 391 (1995).
19. G. Mosialos *et al.*, *Am. J. Pathol.* **148**, 593 (1996).
20. S. S. Frankel *et al.*, unpublished data.
21. D. C. Kalter *et al.*, *J. Immunol.* **146**, 3396 (1991); J. Kanitakis *et al.*, *AIDS Res. Hum. Retroviruses* **5**, 293 (1989); H. Muller *et al.*, *Res. Virol.* **144**, 59 (1993); A. Gianetti *et al.*, *J. AIDS* **6**, 329 (1993).
22. M. Pope, M. G. H. Betjes, H. Hirmand, L. Hoffman, R. M. Steinman, *J. Invest. Dermatol.* **104**, 11 (1995).
23. S. Jurriaans *et al.*, *Virology* **204**, 223 (1994).
24. A. I. Spira *et al.*, *J. Exp. Med.* **183**, 215 (1996).


25. Supported by NIH grant AI24775, the Dorothy Schiff Foundation, the Norman and Rosita Winston Fellowship Program (M.P.), the Direct Effect AIDS Researcher Program, Army research and development contract 90MM0604, and an American Registry of Pathology research grant. We thank R. Virmani for encouragement. The opinions and assertions contained herein are the private views of the authors and are not to be construed as official or as reflecting the views of the Departments of the Navy, Army, or Defense.

1 November 1995; accepted 1 February 1996


# Equilibrium-Point Control Hypothesis Examined by Measured Arm Stiffness During Multijoint Movement


Hiroaki Gomi and Mitsuo Kawato



For the last 20 years, it has been hypothesized that well-coordinated, multijoint movements are executed without complex computation by the brain, with the use of springlike muscle properties and peripheral neural feedback loops. However, it has been technically and conceptually difficult to examine this "equilibrium-point control" hypothesis directly in physiological or behavioral experiments. A high-performance manipulandum was developed and used here to measure human arm stiffness, the magnitude of which during multijoint movement is important for this hypothesis. Here, the equilibrium-point trajectory was estimated from the measured stiffness, the actual trajectory, and the generated torque. Its velocity profile differed from that of the actual trajectory. These results argue against the hypothesis that the brain sends as a motor command only an equilibrium-point trajectory similar to the actual trajectory.


Humans can extend their arms toward a visual target effortlessly. However, recent studies in robotics (*1*) and computational neuroscience (*2*) have revealed that because of nonlinear interaction forces between the arm's many degrees of freedom, complex computations are required to generate the motor commands necessary to realize a desired trajectory faithfully. Although this statement is generally true regarding the whole computational machinery including the brain, the spinal cord, reflex loops, and muscles, a widely accepted premise is that the brain avoids such complex computations because it can rely on the beneficial elastic properties inherent in muscles and peripheral reflex loops. Numerous theories and models have been developed along these lines (*3–6*), and some can be summarized as the following control scheme: The brain sends an "equilibrium-point trajectory," which is similar to the desired trajectory, to the periphery as a motor command. The equilibrium-point trajectory is a time series of equilibrium points, each of which would be realized because of the mechanically stable elastic properties of the muscles and reflexes if the motor command at some instant were maintained indefinitely. Because the limb will realize a trajectory that is similar to the equilibrium-point trajectory and because it is known (*7*) that arm movements are well approximated by simple geometric curves, it follows that the equilibrium-point trajectory should be simple too. These simple equilibrium-point trajectories can be planned without complex computation.

Few researchers doubt that the springlike properties of the neuromuscular system are of importance in maintaining stable posture (*8*). The crucial question, however, is how far this system by itself suffices to generate movement. We investigated whether the equilibrium-point trajectory reconstructed from humans was similar to their actually realized trajectories, one of the major assumptions of the equilibrium-point control hypothesis (*9*).

Several simulation studies conducted to investigate this question (*4–6*, *10*) revealed the critical importance of the magnitude of arm stiffness during movement. That is, if the arm stiffness during movement is large [on average, 67.9 N m/rad for the shoulder and 78.0 N m/rad for the elbow in (*4*)], then the equilibrium-point trajectory is similar to the actual one, and complex computations are thus not necessary. On the other hand, if the arm stiffness is small [19.5 N m/rad for the shoulder and 15 N m/rad for the elbow in (*10*)], the two trajectories are very different and computation is necessary for calculating this complicated equilibrium-point trajectory. Thus, it is critical to measure arm stiffness during multijoint movement.


H. Gomi, NTT Basic Research Labs, Information Science Research Lab, Wakamiya 3-1, Morinosato, Atsugi, Kanagawa-pref., Japan. E-mail: gomi@idea.brl.ntt.jp
M. Kawato, ATR Human Information Processing Research Labs, Hikaridai 2-2, Seika-cho, Soraku-gun, Kyoto-pref., Japan. E-mail: kawato@hip.atr.co.jp

Unfortunately, this is much more difficult than conducting measurements during posture maintenance (*11*) or during single-joint movement (*12, 13*), and data from these other conditions cannot be used. The stiffness measurement invokes application of external forces to the arm by a manipulandum and measurement of the resulting trajectory perturbations. If the perturbation is too large or the manipulandum is too heavy, test participants cannot complete natural point-to-point movements. On the other hand, if the perturbation is too small, a reliable estimation cannot be accomplished. To circumvent these problems, we developed the parallel link drive air-magnet floating manipulandum (PFM) (Fig. 1). It is fast and light enough to minimize movement interference but strong enough to transmit large forces and rigid enough to produce reliable estimates.

Another difficulty in such measurements concerns the nonlinear dynamics of the arm. If inertial parameters, which change in time during movement, are directly estimated in joint or Cartesian coordinates (*14*), many independent inertial parameters must be estimated at different postures, which may lead to an unreliable estimation. We developed a new estimation method that requires only three parameters of the arm dynamics for the entire movement duration by assuming that the human arm can be modeled as a two-link rigid body (*15*). The applied external forces were decomposed into arm dynamics and muscle-generated force, the latter of which consists of viscosity and elastic force. The estimated coefficient of the position relating to the elastic force is the required stiffness (*15*).

Three test participants (two males and one female, 26 to 34 years old, right-handed) participated in this study. Each person sat in front of the PFM while strapped securely to the chair back (Fig. 1). Small force perturbations lasting for a brief period (about 0.2 s) pushed the person's hand and then pulled it back (6 to 8 mm) in eight directions at nine times before, during, and after movements. These 72 (8 × 9) different perturbations were applied within each set in random order. Eight data sets were recorded for each person, excluding failed trials (Fig. 1). Test participants were instructed to follow the target movement with high accuracy (<3 cm), but the target was deliberately extinguished for 0.4 s after the perturbation was initiated. Test participants could not tell the direction, and sometimes even the time, of the perturbation. Thus, it was very unlikely that they voluntarily changed their motor commands in response to different perturbations. The squares of the correlation coefficients between the reconstructed applied external torques and the real ones were between 0.85 and 0.98 for 27 (9 times × 3 people) estimations, which indicates the high reliability of the method.

The upper row of Fig. 2 shows the stiffness ellipses calculated from these data during multijoint movement. The ellipses represent the direction and magnitude of elastic, resisting forces to unit-length position perturbations in all directions. The long axis of each ellipse represents maximum force, indicating the greatest stiffness. Conversely, the short axis represents minimum force, indicating the least stiffness. Because 0.3 s of data were used to estimate stiffness after the perturbation was initiated, both the muscle's intrinsic elastic property and its short-latency reflexes contributed to the estimated stiffness. The numbers attached to these ellipses indicate the nine times of estimation, each separated by 0.2 s before the movement (1 and 2), at the movement start (3), during (4 to 7), and then after (8 and 9) the movement. At the first perturbation time, the stiffness ellipses were thin with their long axis oriented toward the shoulder, which is a common feature of stiffness ellipses during posture maintenance (*11*). The ellipses started to enlarge around movement start (2 to 4). The areas of the ellipses (*11*) during the movement (4 to 7) were on average 7.2 times larger than those during relaxed, corresponding postures. This increase most likely reflects the muscle tension required to execute the movement. Along with the size change, the shape of the ellipses during movement (4 to 7) became slightly thicker than those while posture was maintained [the ratio of long and short axes of movement (2.7 ± 0.6) was significantly different from those of posture (5.1 ± 2.3)].

The lower row in Fig. 2 shows the temporal changes of shoulder and elbow joint stiffness and two-joint stiffness ($R_{es}$, calculating elbow torque from shoulder rotation) during movement, with their 90% confidence intervals. The shoulder stiffness increased around movement start, slightly decreased in the middle of the movement, then increased again around movement end. This is similar to data from elbow single joint movements (*13*). The timing of the stiffness decrease might correspond to the switch from shoulder extensor activation to shoulder flexor activation for decelerating the shoulder extension movement. The ratio between the stiffness components (shoulder, elbow, and double joints) changed dynamically during movement. This change was not observed while posture was maintained (*11*), which indicates that the activation pattern of the muscles was greatly changed during movement. In contrast to single joint cyclic movements (*12*), the joint stiffness values during movement were always larger than those during corresponding postures. All stiffness components decreased after

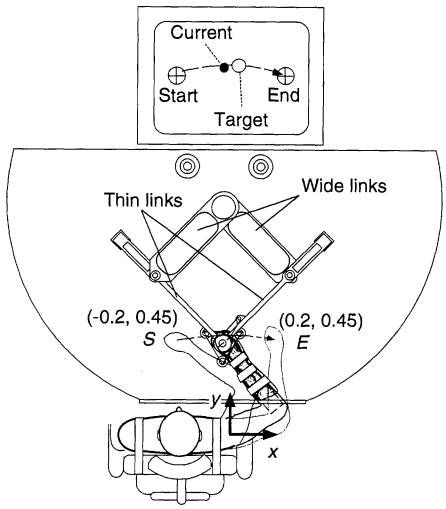


**Fig. 1.** The parallel link drive air-magnet floating manipulandum (PFM) and the experimental setup for measuring human arm stiffness. The two thin links are driven by two wide links, and the wide links are directly driven by two powerful electric motors placed under the table. The handle of the manipulandum (each person's hand position) is supported by an air-magnet floating mechanism to prevent the person's arm from leaning and to avoid friction. Because of this special mechanism and the parallel link architecture, no bending force is imposed on the links, and the links can be very light and thin but still rigid enough within the horizontal plane. The handle and the supporting beam can be rotated freely at the top of the links within the horizontal plane. The participant's hand position (handle center) was measured by the joint position sensors of the PFM, and the force exerted by the PFM on the hand was measured by a force sensor placed between the handle and the PFM links. The PFM was controlled by a digital signal processor (0.5 ms per cycle) to reduce the dynamical effects of the PFM on each person's hand. The effective mass and viscosity were 0.65 kg and 4.40 N/(m/s), respectively. The *x* axis indicates the rightward direction, and the *y* axis indicates the frontal direction away from the body. The origin is the shoulder position. The right forearm was placed in a molded plastic cuff tightly coupled with the handle (the same movements of the handle, the cuff, and the arm were confirmed in advance by an optical position sensor) and supported in the vertical direction by the beam. The hand was able to move freely in any direction within the horizontal plane at shoulder level. Each participant moved his or her hand from the start position displayed as a crossed circle on a cathode ray tube (CRT) (top), which corresponds to position $S = -0.2$ m, 0.45 m on the hand plane, to the end position (crossed circle), which corresponds to position $E = 0.2$ m, 0.45 m on the hand plane. The current hand position was displayed by a cursor with a filled circle on the CRT. The movement duration of 1 s was determined by beeping sounds, and the movement magnitude was 0.4 m. To reduce the trajectory variance, a reference hand trajectory, which itself consisted of each person's averaged trajectory from pre-trials, was also displayed by a moving target (open circle) on the CRT. Only those trajectories close to the reference trajectory (<3 cm at each time step) were recorded for data analysis.

movement. The elbow joint stiffness (range, 3 to 14 N m/rad) during single joint movement explored by different perturbation patterns (random and step in several amplitudes) (*12, 13*) did not differ considerably from our results here (range, 5 to 21 N m/rad). Slightly greater stiffness in multijoint movement might be ascribed to forces of interaction between the shoulder and the elbow.

The equilibrium-point trajectories for the three participants here were calculated from actual trajectories, generated muscle torques, and the estimated joint stiffness (Fig. 3) (*16*). Figure 3 shows the *x* axis (main movement component) position as a function of movement time and the tangential velocity profiles. The dash-dot curves indicate the actual trajectory, and the solid curves show the equilibrium-point trajectory. The mean and standard deviation of the maximum difference in the equilibrium position calculated from 90% confidence intervals of the estimated stiffness and the viscosity are 0.0050 m and 0.0063 m for nine positions and three participants, which indicates the high reliability of the calculation. The equilibrium position first led the actual position to generate the accelerating torque, then fell behind the actual position to generate the decelerating torque. All of the velocity profiles of the equilibrium-point trajectory had multiple peaks, which are very different from the actual velocity profiles. The equilibrium-point velocity, in particular, increased rapidly and peaked just after the initiation of the movement. These results imply that the brain needs to acquire some internal models of the controlled objects (*17*).

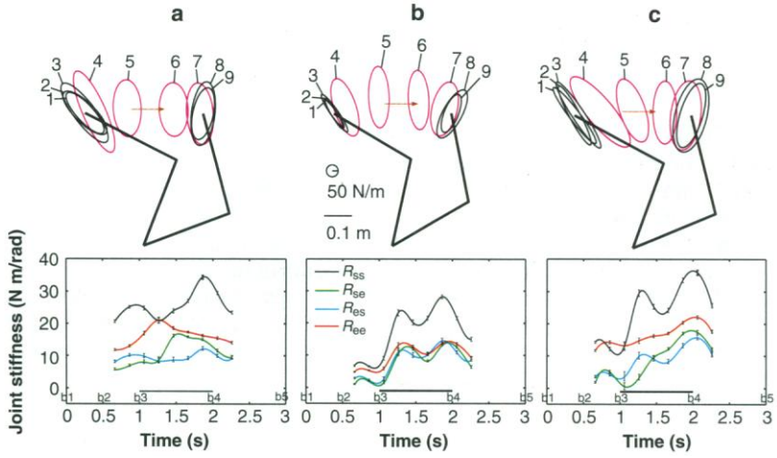


**Fig. 2.** Stiffness ellipses (top) and joint stiffness values of shoulder ($R_{ss}$, black), elbow ($R_{ee}$, red), and two-joints ($R_{se}$, green, and $R_{es}$, blue) (bottom) for test participants a, b (female), and c. At the top, the start and end arm configurations are shown by stick figures in the (*x, y*) coordinates defined in Fig. 1. The center of each stiffness ellipse is located at the hand position for the corresponding arm configuration during the movement. The ellipses colored magenta denote the stiffness during movement (4 through 7). First, joint stiffness values were calculated as described (*15*); then, to draw the ellipses, we calculated the hand stiffness by a coordinate transformation. Time 0 at the bottom denotes the first beeping sound (b1). The participants were instructed to start from position *S* (see Fig. 1) at the third beep (b3), to stop in position *E* at the fourth beep (b4), and to hold their hands there until the fifth beep (b5). The thick horizontal line denotes the movement duration. The perturbation force used for measuring the third ellipse began 0.1 s before b3 (movement start), and that for the eighth ellipse began 0.1 s before b4 (movement end). Each error bar denotes the 90% confidence interval of each estimate.

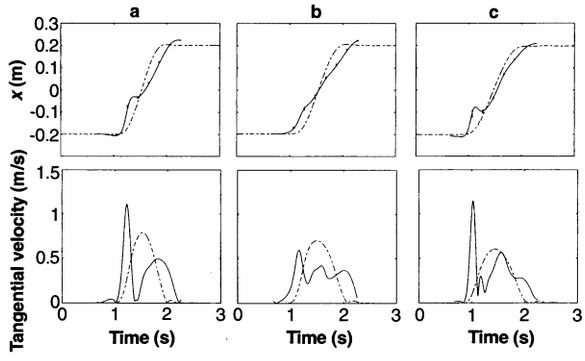


**Fig. 3.** The *x* axis (main movement component) position of the equilibrium-point trajectory as a function of movement time with the error bars calculated from 90% confidence interval (solid curves at the top), and the tangential velocity profiles of the equilibrium-point trajectories (solid curves at the bottom) for test participants a, b, and c. The dash-dot curves indicate the actual trajectory in each figure. According to the equilibrium-point control hypothesis (*3, 4*), the equilibrium point ($\mathbf{q}_{eq}$) represented in joint-angle coordinates is calculated as follows:

$$\mathbf{q}_{eq} = \mathbf{R}^{-1}(\tau_{in} + \mathbf{D}\dot{\mathbf{q}}) + \mathbf{q} \quad (3)$$

Other notations are the same as in (*15*). This equation is derived from the linear approximation of $\tau_{in}$ in Eq. 1 around the actual trajectory just as in Eq. 2 such as $\tau_{in} = \mathbf{R}(\mathbf{q}_{eq} - \mathbf{q}) - \mathbf{D}\dot{\mathbf{q}}$. Note that $\tau_{in} = 0$ holds while $\mathbf{q} = \mathbf{q}_{eq}$, $\dot{\mathbf{q}} = 0$ from the definition of the equilibrium point. In Eq. 3, **R** and **D** were already estimated, and **q** and $\dot{\mathbf{q}}$ are simply the unperturbed, control trajectory and its velocity, respectively. $\tau_{in}$ can be calculated from the difference of the left side of Eq. 1 and the measured $\tau_{ext}$. Consequently, the equilibrium-point trajectory can be calculated from experimental data. It was computed every 0.05 s from **R** and **D**, which were interpolated between estimated values at every 0.2 s by a third-order spline. The equilibrium hand position in Cartesian coordinates was derived, by a coordinate transformation, from that in joint coordinates.

## REFERENCES AND NOTES


1. R. P. Paul, *Robot Manipulators: Mathematics, Programming, and Control* (MIT Press, Cambridge, MA, 1981); J. M. Hollerbach, in *Robotics Science,* M. Brady, Ed. (MIT Press, Cambridge, MA, 1989), pp. 378–431.
2. M. Kawato, in *Attention and Performance XIV,* D. Meyer and S. Kornblum, Eds. (MIT Press, Cambridge, MA, 1992), pp. 821–849.
3. A. G. Feldman, *Biophysics* **11**, 565 (1966); E. Bizzi, A. Polit, P. Morasso, *J. Neurophysiol.* **39**, 435 (1976); A. Polit and E. Bizzi, *ibid.* **42**, 183 (1979); E. Bizzi, N. Accornero, W. Chapple, N. Hogan, *J. Neurosci.* **4**, 2738 (1984); N. Hogan, *ibid.*, p. 2745; A. G. Feldman, *J. Mot. Behav.* **18**, 17 (1986).
4. T. Flash, *Biol. Cybern.* **57**, 257 (1987).
5. J. R. Flanagan, D. J. Ostry, A. G. Feldman, *J. Mot. Behav.* **25**, 140 (1993).
6. J. McIntyre and E. Bizzi, *ibid.*, p. 193.
7. J. A. S. Kelso, D. L. Southard, D. Goodman, *Science* **203**, 1029 (1979); P. Morasso, *Exp. Brain Res.* **42**, 223 (1981); W. Abend, E. Bizzi, P. Morasso, *Brain* **105**, 331 (1982); T. Flash and N. Hogan, *J. Neurosci.* **5**, 1688 (1985); Y. Uno, M. Kawato, R. Suzuki, *Biol. Cybern.* **61**, 89 (1989).
8. T. R. Nichols and J. C. Houk, *J. Neurophysiol.* **39**, 119 (1976); N. Hogan, *Biol. Cybern.* **52**, 315 (1985); J. M. Winters, in *Multiple Muscle Systems: Biomechanics and Movement Organization,* J. M. Winters and S. L.-Y. Woo, Eds. (Springer-Verlag, New York, 1990), pp. 69–93.
9. Special issue on Controversies in Neuroscience I: Movement Control, *Behav. Brain Sci.* **15** (1992); special issue on Modeling the Control of Upper Limb Movement, *J. Mot. Behav.* **25** (1993).
10. M. Katayama and M. Kawato, *Biol. Cybern.* **69**, 353 (1993).
11. F. A. Mussa-Ivaldi, N. Hogan, E. Bizzi, *J. Neurosci.* **5**, 2732 (1985); T. Flash and F. A. Mussa-Ivaldi, *Exp. Brain Res.* **82**, 315 (1990); J. M. Dolan, M. B. Friedman, M. L. Nagurka, *IEEE Trans. Syst. Man Cybern.* **23**, 698 (1993); F. Lacquaniti, M. Carrozzo, N. A. Borghese, *J. Neurophysiol.* **69**, 1443 (1993); T. Tsuji, P. G. Morasso, K. Goto, K. Ito, *Biol. Cybern.* **72**, 475 (1995).
12. D. J. Bennett, J. M. Hollerbach, Y. Xu, I. W. Hunter, *Exp. Brain Res.* **88**, 433 (1992).
13. D. J. Bennett, *ibid.* **95**, 488 (1993).
14. H. Gomi, Y. Koike, M. Kawato, *Proc. 14th IEEE Eng. Med. Biol. Soc.* **4**, 1628 (1992).
15. The human arm (upper arm and forearm) dynamics within the horizontal plane can be expressed by the following nonlinear dynamics equation:

$$\mathbf{I}(\mathbf{q})\ddot{\mathbf{q}} + \mathbf{H}(\dot{\mathbf{q}},\mathbf{q}) = \tau_{in}(\dot{\mathbf{q}},\mathbf{q},\mathbf{u}) + \tau_{ext} \quad (1)$$

Here **q** is the state vector consisting of shoulder and elbow joint angles ($\mathbf{q} = [\theta_{shoulder}, \theta_{elbow}]^T$), $\dot{\mathbf{q}}$ and $\ddot{\mathbf{q}}$ are its velocity and acceleration, respectively. **I** denotes the position-dependent inertia matrix (2 × 2), and **H** denotes Coriolis and centripetal forces. The left side of this equation represents the link dynamics

of the arm, including the cuff and the supporting beam. The right side is the torque imposed on this composite object and is the sum of muscle-generated torque ($\tau_{in}$) and the torque applied by the PFM ($\tau_{ext}$). $\tau_{in}$ depends nonlinearly on muscle length (a function of $\mathbf{q}$) and velocity (a function of $\dot{\mathbf{q}}$) as well as on the descending motor commands ($\mathbf{u}$). $\tau_{ext}$ can be measured by the force sensor attached to the handle of the PFM. By linearizing Eq. 1 around the unperturbed, control trajectory, the following variational equation can be derived:

$$\mathbf{I}\delta\ddot{\mathbf{q}} + \frac{\partial \mathbf{H}}{\partial \dot{\mathbf{q}}}\delta\dot{\mathbf{q}} + \left(\frac{\partial \mathbf{I}\ddot{\mathbf{q}}}{\partial \mathbf{q}} + \frac{\partial \mathbf{H}}{\partial \mathbf{q}}\right)\delta\mathbf{q} = \frac{\partial \tau_{in}}{\partial \dot{\mathbf{q}}}\delta\dot{\mathbf{q}} + \frac{\partial \tau_{in}}{\partial \mathbf{q}}\delta\mathbf{q} + \delta\tau_{ext} \equiv -\mathbf{D}\delta\dot{\mathbf{q}} - \mathbf{R}\delta\mathbf{q} + \delta\tau_{ext} \quad (2)$$

where $\delta\mathbf{q}$, $\delta\dot{\mathbf{q}}$, and $\delta\ddot{\mathbf{q}}$ are positional, velocity, and acceleration perturbations, respectively, caused by imposed force perturbation $\delta\tau_{ext}$ by the PFM. In the analysis, they were, respectively, measured as the difference between the perturbed trajectory and the control trajectory (the average of perturbed trajectories) and its first and second derivatives. Offsets in all quantities relative to the control trajectory at the start of a perturbation were eliminated. The force perturbation was derived as the difference between the perturbed and the control external torque patterns. **D** and **R** denote viscosity and stiffness matrices, respectively. If we apply a least-squared error estimation method to this variational equation, then the time-variant 2 × 2 matrices for the acceleration coefficient (inertia), velocity coefficient (viscosity), and position coefficient (stiffness) can be estimated, but for the inertial matrix 36 (4 components × 9 times), independent parameters must be estimated. Because the left sides of both Eqs. 1 and 2 can be linearized with respect to the physical parameters of the links, only three independent parameters are sufficient to specify them. Those are uniquely determined from the physical characteristics of the links. These three parameters were preestimated with the use of all the data sets measured for each person, then viscosity and stiffness were estimated at each perturbation time (*18*).

16. At least three objections might exist concerning our way of calculating the equilibrium-point trajectory. One is to assert that the nonlinear muscle length-tension curve [especially the exponentially increasing, accelerating nonlinearity (*5*)] can produce large forces even with the equilibrium-point trajectory close to the actual trajectory. Our approach, a linearization of the nonlinear length-tension curve, may overestimate the difference between the equilibrium and actual positions. By recalling that arm stiffness is measured around the actual trajectory, not around the equilibrium-point trajectory, we can actually show the opposite. Let us define the following single joint stiffness values as the derivative of $\tau_{in}$ with respect to $\theta$ but estimated at the actual position $\theta$ and the equilibrium position $\theta_{eq}$: $R \equiv -\partial\tau_{in}(\theta)/\partial\theta$ and $R_{eq} \equiv -\partial\tau_{in}(\theta_{eq})/\partial\theta_{eq}$. From the accelerating nonlinearity of $\tau_{in}$, we can assert that $R_{eq} < R$, and $|\tau_{in}/R| < |\theta_{eq}^{real} - \theta|$. Here, $\theta_{eq}^{real}$ denotes the real equilibrium position considering the nonlinearity of the muscle length-tension curve. The second possible criticism is a new version of the equilibrium-point control hypothesis that uses not only the position information of the desired trajectory ($\theta_d$) but also its velocity wave form for generating muscle torque, such as $\tau_{in} = R(\theta_d - \theta) + D(\dot{\theta}_d - \dot{\theta})$ (*6*). For the case of single joint movement, it was demonstrated that with this new version a simple trajectory can control relatively fast movement (*6*). However, we found that even with this new version, a simple straight equilibrium-point trajectory cannot control multijoint movements (*10*) [N. Schweighofer, thesis, University of Southern California (1995)]. This is reasonable because the viscosity force is always one order of magnitude smaller than the elastic force in our experiments. The third possible criticism is that for some reason our measured stiffness values are different from those used under the equilibrium-point control hypothesis. For example, stiffness value estimations depend on the perturbations used. In our exploratory experiments, we found that the measured stiffness values became smaller for larger amplitude perturbations and for lower temporal frequency (*12, 13*). Because the equilibrium-point trajectory seems to be larger in amplitude and lower in temporal frequency than the currently used perturbation patterns, our stiffness estimation may be an overestimation. Consequently, our main conclusion here still holds.


17. M. Kawato, K. Furukawa, R. Suzuki, *Biol. Cybern.* **57**, 169 (1987); M. Kawato and H. Gomi, *Trends Neurosci.* **15**, 445 (1992); M. Shidara, K. Kawano, H. Gomi, M. Kawato, *Nature* **365**, 50 (1993).
18. H. Gomi and M. Kawato, *Technical Report No. ISRL-95-4* (NTT Basic Research Labs, Information Science Research Lab, 1995).


19. We thank M. Honda and K. Ishii of NTT and Y. Tohkura of ATR for their continuing encouragement; F. Pollick and S. Schaal for improving the manuscript; and N. Imamura and E. Nagaoka of KOBELCO and T. Yoshioka of CSK Corp. for their technical support. Supported by Human Frontier Science Program grants to M.K.

10 October 1995; accepted 5 February 1996


# Role of the Nuclear Transport Factor p10 in Nuclear Import


Ulf Nehrbass and Günter Blobel*



**The nuclear import factor p10 was cloned from *Saccharomyces cerevisiae* and found to be essential. The protein p10 can bind directly to several peptide repeat–containing nucleoporins. It also binds to the guanosine triphosphatase (GTPase) Ran in its guanosine diphosphate (GDP)–bound form and to karyopherin β. Assembly of the karyopherin heterodimer on immobilized nucleoporin yielded cooperative binding of p10 and Ran-GDP. Addition of GTP to this pentameric complex led to dissociation of karyopherin α, presumably via in situ formation of Ran-GTP from Ran-GDP. Thus, p10 appears to coordinate the Ran-dependent association and dissociation reactions underlying nuclear import.**


Protein import across the nuclear pore complex (NPC) is mediated by at least four soluble factors. These cytosolic factors restore nuclear import in cells depleted of cytosol by digitonin permeabilization. Two of these factors form a heterodimer termed karyopherin (*1–9*). Karyopherin α binds to nuclear localization sequence (NLS)–containing proteins (*2, 10–12*), and karyopherin β mediates docking to peptide repeats of nucleoporins (*1, 10, 13*). The GTPase Ran (*14, 15*) and an additional protein referred to as p10 (*10, 16, 17*) are required for subsequent translocation of the docked NLS protein into the nucleoplasm (*1, 10, 14, 16*) along with karyopherin α. Karyopherin β remains bound to the NPC (*8, 10*). The role of p10 in the translocation reaction is not clear. It can bind to the nucleoporin p62 (*17*) and appears to form a complex with Ran in the cytosol (*16*), although a direct interaction has not yet been demonstrated.

*Saccharomyces cerevisiae* contains a conserved set of import factors (*18*). In solution-binding assays (*19*), the karyopherin αβ heterodimer (Kap60α and Kap95β) associates with either NLS protein or nucleoporin FXFG (phenylalanine-X-phenylalanine-glycine) repeats in a cooperative fashion. Moreover, Ran-GTP dissociates the heterodimeric αβ complex by binding to karyopherin β, thus releasing the karyopherins from the nucleoporin docking site. Ran-GDP binds to karyopherin β with much lower affinity and does not induce dissociation (*20*). As docking and release are principal functions of soluble factors, nuclear translocation has been proposed to result from repeated docking and release reactions along an array of docking sites on the NPC fibers (*13*). Because Ran-GTP is the major

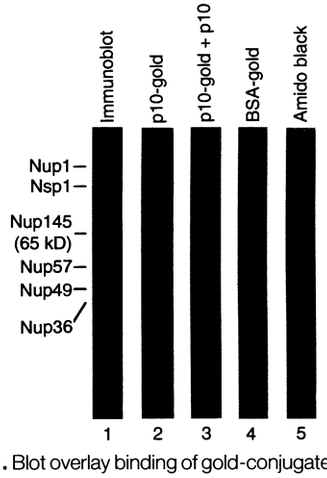


**Fig. 1.** Blot overlay binding of gold-conjugated p10 to a subset of nucleoporins. Proteins of yeast nuclear envelopes (*26, 28*) were separated by SDS-PAGE and transferred to nitrocellulose. The protein pattern is shown by Amido black staining (lane 5). Strips were probed with p10-gold conjugate (*27*) in the absence (lane 2) or presence (lane 3) of a 200-fold excess of nonconjugated p10, or were probed with a BSA-gold conjugate (lane 4). Another strip (lane 1) was probed with monoclonal antibodies 14 and 192 (*29*), which recognize the peptide repeat motifs of various nucleoporins, and with an affinity-purified antibody against Nup36 (*31*).


Laboratory of Cell Biology, Howard Hughes Medical Institute, Rockefeller University, New York, NY 10021, USA.

*To whom correspondence should be addressed. E-mail: blobel@rockvax.rockefeller.edu